IEICE TRANSACTIONS

on Communications

VOL. E100-B NO. 8
AUGUST 2017



A PUBLICATION OF THE COMMUNICATIONS SOCIETY

The Institute of Electronics, Information and Communication Engineers
Kikai-Shinko-Kaikan Bldg., 5-8, Shibakoen 3chome, Minato-ku, TOKYO, 105-0011 JAPAN

IEICE TRANS. COMMUN., VOL.E100–B, NO.8 AUGUST 2017

PAPER Special Section on Radio Access Technologies for 5G Mobile Communications System

# Cooperative Distributed Antenna Transmission for 5G Mobile Communications Network

**Fumiyuki ADACHI**[†a)], ***Fellow***, **Amnart BOONKAJAY**[†], **Yuta SEKI**[†], **Tomoyuki SAITO**[†], **Shinya KUMAGAI**[†], ***and*** **Hiroyuki MIYAZAKI**[†], ***Members***

**SUMMARY** In this paper, the recent advances in cooperative distributed antenna transmission (CDAT) are introduced for spatial diversity and multi-user spatial multiplexing in 5G mobile communications network. CDAT is an advanced version of the coordinated multi-point (CoMP) transmission. Space-time block coded transmit diversity (STBC-TD) for spatial diversity and minimum mean square error filtering combined with singular value decomposition (MMSE-SVD) for multi-user spatial multiplexing are described under the presence of co-channel interference from adjacent macro-cells. Blind selected mapping (blind SLM) which requires no side information transmission is introduced in order to suppress the increased peak-to-average signal power ratio (PAPR) of the transmit signals when CDAT is applied. Some computer simulation results are presented to confirm the effectiveness of CDAT techniques.

***key words:*** *5G mobile communications network, distributed antenna network, cooperative signal transmission, space-time block coding, multi-user communication, signal peak suppression*

## 1. Introduction

After 35 years from its birth in Dec. 1979 in Japan, mobile communications networks have evolved into the 4th generation (4G) networks in 2015 [1]–[3]. In 4G (called long-term evolution (LTE)-Advanced), high-quality video communications and close-to-1Gbps broadband data services have been becoming more popular. The cellular networks reuse the same frequency to utilize the limited available bandwidth efficiently. However, this frequency reuse introduces the co-channel interference (CCI), from adjacent cells, that limits the transmission quality. For cell-edge users, the received signal power reduces due to large path loss while strong CCI is received (i.e., the received signal-to-interference plus noise power ratio (SINR) degrades significantly) and therefore, we will not be able to achieve the required transmission quality. To solve this problem, 4G networks have adopted the coordinated multi-point (CoMP) transmission technique [4].

In the 5$^{th}$ generation (5G) networks, we expect much broader data services (> 1 Gbps/user). Recently, the development of 5G networks achieving higher spectrum efficiency (SE) and energy efficiency (EE) than 4G networks is on-going worldwide [5]. In Japan, the research and development project for realizing the 5G mobile communications networks started in Sept. 2015 [6]. One promising approach is a distributed antenna small-cell network [7]–[9] that deploys a number of distributed antennas over a traditional macro-cell to exploit the spatial domain more efficiently. For efficient signal transmission using distributed antennas, the authors have been studying the cooperative distributed antenna transmission (CDAT) for spatial diversity and multi-user spatial multiplexing. We view CDAT as an advanced version of CoMP in 4G networks.

For spatial diversity, the authors proposed a space-time block coded transmit diversity (STBC-TD) jointly used with maximal ratio transmit frequency-domain equalization (MRT-FDE) for the orthogonal frequency division multiplexing (OFDM) downlink transmission [10] and that with receive minimum mean square error based FDE (MMSE-FDE) for the single-carrier (SC) uplink transmission [11]. For multi-user spatial multiplexing, the authors proposed an MMSE filtering combined with singular value decomposition (MMSE-SVD) for both OFDM downlink and SC uplink transmissions [12]–[15]. The spatial diversity aims at improving the macro-cell edge users' link capacity while the multi-user spatial multiplexing improving the capacity of users in a good propagation condition. In distributed antenna small-cell networks, we can utilize high frequency bands, e.g., millimeter wave bands, due to the short distance radio link (resulting in reduced path loss). In such high frequency bands, abundant bandwidths remain unused; therefore, we can significantly increase the data rate. However, the application of CDAT increases the peak-to-average signal power ratio (PAPR) of transmit signal (the reason why the CDAT increases the PAPR will be described briefly in Sect. 3.3). Hence, some PAPR reduction techniques will be necessary for transmit power amplifiers of battery-operated mobile terminals. The authors proposed blind selected mapping (blind SLM) which does not require the transmission of side information (such as phase rotation sequence information) [16]–[18]. Blind SLM technique for STBC-TD transmission was also presented in [19]. This paper provides a comprehensive report of the above recent advances in CDAT techniques. The performances of those CDAT techniques are evaluated and compared under the same simulation condition. Moreover, transmit MMSE filtering which considers CCI for MMSE-SVD technique is newly proposed.

The rest of paper is organized as follows. Section 2 introduces the distributed antenna small-cell network. Then, we introduce the recent advances in CDAT techniques and

Manuscript received September 2, 2016.
Manuscript revised December 16, 2016.
Final manuscript received February 8, 2017.

[†]The authors are with Tohoku University, Sendai-shi, 980-8579 Japan.
a) E-mail: adachi@ecei.tohoku.ac.jp

DOI: 10.1587/transcom.2016FGP0019

present mathematical signal representations for those CDAT techniques in Sect. 3. Section 4 presents computer simulation results of CDAT to confirm its effectiveness in multi-macro-cell environment. Section 5 offers concluding remarks.

*Notations*: $E[\cdot]$, $[\cdot]^T$, $[\cdot]^*$, and $[\cdot]^H$ represent ensemble average, transpose, complex conjugate, and Hermitian transpose operations, respectively. $(x)^+$ represents $max(0, x)$. $\mathbf{I}_N$ is an $N \times N$ identity matrix.

## 2. Distributed Antenna Small-Cell Network

The design of the mobile communications network is based on the cellular concept [20] to effectively utilize the limited available bandwidth and accordingly the area SE (ASE) (bps/Hz/km$^2$). The cellular concept is that the service area is divided into small areas called cells, each of which is covered by a base station (BS). The spatially separated BSs reuse the same frequency as long as the CCI is kept below a predetermined allowable level. Improving the ASE is one important challenge for mobile communications networks. Another challenge for 5G is improving the EE (bits/Joule) since increasing the data rates leads to increasing the transmit signal power (this becomes a serious problem in particular for battery operated mobile terminals).

One promising approach for simultaneous improvement of the ASE and the EE is a small-cell structured network. Reducing the BS coverage area (i.e., small-cell) enables the same frequency to be reused more densely in the same service area and accordingly the ASE can improve. The short distance communications allow the transmit signal power significantly lowered, thereby the EE improves. However, frequent handover may happen in order to enable the continuous communication while a user is traveling or even walking and may increase the control signal traffic.

There are two main approaches to avoid frequent handover. One is to deploy a number of distributed antennas over a macro-cell covered by a BS [21], [22]. In this paper, we call this network the distributed antenna small-cell network [7]–[9] (or a distributed massive multi-input multi-output (distributed massive MIMO) network). The other approach is to introduce massive MIMO [23] (or a centralized massive MIMO). We can replace the handover problem with the selection of appropriate distributed antennas for the former network and with a selection of beams for the latter network within the same BS. Possible advantage of using distributed antennas over centralized massive MIMO is its capability of alleviating problem raised by the shadowing loss and path loss.

Figure 1 illustrates the conceptual structure of distributed antenna small-cell network. Each distributed antenna and macro-cell BS (MBS) are connected by optical fiber link. MBS performs radio signal processing for signal transmission and reception, whilst the distributed antennas near a user equipment (UE) form a user-centric small-cell and perform CDAT.

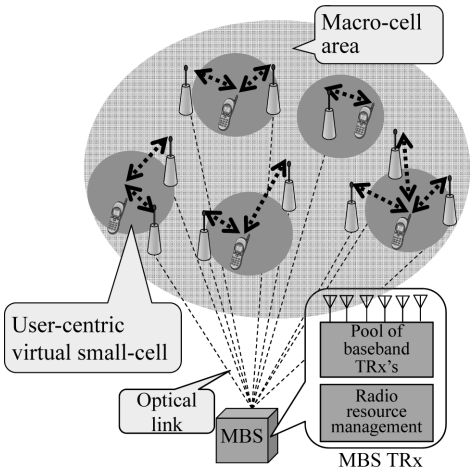


**Fig. 1** Conceptual structure of distributed antenna small-cell network (only single macro-cell area covered by single MBS is illustrated).

## 3. Cooperative Distributed Antenna Transmission (CDAT)

The broadband channel is severely frequency-selective. Therefore, it is necessary to combine some powerful equalization technique, e.g., FDE used in LTE/LTE-A, with CDAT to tackle the frequency-selectivity of the channel. FDE requires the channel estimation to acquire the channel state information (CSI). In the time division duplex (TDD) transmission scheme, the same frequency is used for both uplink (UE→MBS) and downlink (MBS→UE) transmissions. Therefore, in TDD, the CSI estimate of uplink can be reused for transmit equalization in the downlink transmission. Because of this reason, FDE for both uplink and downlink transmissions can be done at MBS. In this paper, we consider OFDM and SC block signal transmission for downlink and uplink, respectively. Figure 2 illustrates a simplified transmitter/receiver structure of downlink CDAT. In this section, we firstly present the mathematical signal representation for STBC-TD and then, introduce MMSE-SVD and blind SLM. We adopt frequency-domain signal representation since FDE is used.

Throughout the paper, let $N_{\text{macro}}$ denote the total number of distributed antennas within a macro-cell and $N_{\text{ue}}$ that of UE antennas. We assume that $N_{\text{mbs}}$ ($\leq N_{\text{macro}}$) distributed antennas are selected for data transmission based on a predetermined criterion (which will be described in Sect. 4.1) for data transmission. The number of subcarriers for OFDM and SC transmissions is denoted by $N_c$. Variable $k$ (=0∼$N_c-1$) denotes the subcarrier index and variable $t$ (=0∼$N_c-1$) denotes the time index. Downlink and uplink propagation channel matrices for the $k$th subcarrier are represented by $\mathbf{H}_{\downarrow}(k)$ of size $N_{\text{ue}} \times N_{\text{mbs}}$ and $\mathbf{H}_{\uparrow}(k)$ of size $N_{\text{mbs}} \times N_{\text{ue}}$, respectively. Assuming TDD and stationary fading channel, we have

$$\mathbf{H}_{\downarrow}(k) = \mathbf{H}_{\uparrow}^{T}(k). \tag{1}$$

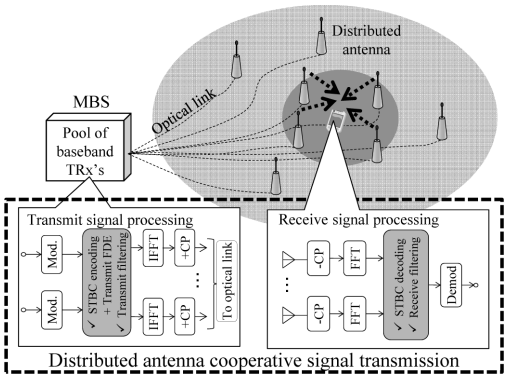


**Fig. 2** A simplified transmitter/receiver structure of downlink CDAT.

Since the available bandwidth is limited, the same frequency needs to be reused in adjacent macro-cells. Therefore, CCI produced by adjacent macro-cells limits the achievable capacity. In the downlink case, signals transmitted from $N_{\mathrm{mbs}}$ distributed antennas of adjacent macro-cell arrives as CCI at $N_{\mathrm{ue}}$ antennas of UE in the macro-cell of interest. CCIs received on $N_{\mathrm{ue}}$ UE antennas can be assumed to be independent zero-mean complex Gaussian variables with the same variance for the given UE locations. On the other hand, in the uplink case, signals transmitted from $N_{\mathrm{ue}}$ antennas of UE of adjacent macro-cell arrives as CCI at $N_{\mathrm{mbs}}$ distributed antennas of macro-cell of interest. Since $N_{\mathrm{mbs}}$ distributed antennas are sufficiently spatially separated, CCIs received on $N_{\mathrm{mbs}}$ distributed antennas can be assumed to be independent complex Gaussian variables with different variances for the given UE locations (the CCI variance varies according to changes in the path loss and shadowing loss). Based on the above discussion, CCI is assumed to have the white power spectrum (i.e., the same power spectrum density over the signal bandwidth). Let $N_0$, $I_{0\downarrow}(u)$, and $I_{0\uparrow}(n_{\mathrm{mbs}})$ denote the power spectrum density of additive white Gaussian noise (AWGN), the CCI power spectrum density received by the $u$th UE, and that received on the $n_{\mathrm{mbs}}$th distributed antenna, respectively. Then, the noise plus CCI can be treated as an equivalent noise having the white power spectrum density of $N_0 + I_{0\downarrow}(u)$ for the downlink and $N_0 + I_{0\uparrow}(n_{\mathrm{mbs}})$ for the uplink. Note that CCI power spectrum density is the same for all $N_{\mathrm{ue}}$ antennas.

In the following, we will develop transmit and receive filter matrices assuming the perfect knowledge of CSI. However, note that the impact of imperfect CSI on STBC-TD and MMSE-SVD is evaluated by computer simulation under a single macro-cell environment (i.e., without CCI).

### 3.1 STBC-TD

Frequency division multi-access (FDMA) is considered for both OFDM downlink and SC uplink. If $U$ UEs access the same MBS simultaneously, the number of subcarriers assigned to each UE becomes $N_c/U$.

Let $N_t$ denote the number of transmit antennas. Using STBC-TD, $J$ symbol blocks of $N_c/U$ symbols each are block encoded into $N_t$ parallel streams of $Q$ blocks each [24], [25]. STBC parameters ($J$, $Q$ and coding rate $R_{\mathrm{STBC}}$) are shown in Table 1 for various values of $N_t$ (note that the number $N_r$ of receive antennas can be arbitrary).

**Table 1** STBC parameters.

| $N_t$ | $N_r$ | $J$ | $Q$ | Coding rate |
|---|---|---|---|---|
| 1 | Arbitrary | 1 | 1 | 1 |
| 2 | | 2 | 2 | 1 |
| 3 | | 3 | 4 | 3/4 |
| 4 | | 3 | 4 | 3/4 |
| 5 | | 10 | 15 | 2/3 |
| 6 | | 20 | 30 | 2/3 |

STBC encoding process can be expressed by matrix $\mathbf{X}(k)$ of size $N_t \times Q$ [26], [27]. Let us assume the OFDM transmission and denote the $k$th data symbol in the $j$th block by $d_j(k)$. For Alamouti STBC ($J$=$Q$=2, $R_{\mathrm{STBC}}$=1), $\mathbf{X}(k)$ of size 2×2 is expressed as

$$\mathbf{X}(k) = \begin{bmatrix} d_0(k) & -d_1^*(k) \\ d_1(k) & d_0^*(k) \end{bmatrix}. \tag{2}$$

The above particular STBC encoding matrix $\mathbf{X}(k)$ of size 2×2 is used in the computer simulation. However, note that in the following mathematical representations, STBC encoding matrix $\mathbf{X}(k)$ of size $N_t \times Q$, which allows $N_t$ up to 6, is considered.

Together with STBC-TD, MRT-FDE and receive MMSE-FDE are used for OFDM downlink transmission ($N_t$=$N_{\mathrm{mbs}}$, $N_r$=$N_{\mathrm{ue}}$) and SC uplink transmission ($N_t$=$N_{\mathrm{ue}}$, $N_r$=$N_{\mathrm{mbs}}$), respectively. In our previous studies [25], [28], [29], STBC encoding matrices when transmit equalization is used were presented for up to 6 receive antennas ($N_{\mathrm{ue}}$=6) (to the best of our knowledge, STBC encoding matrix supporting more than 6 receive antennas has not been discovered yet). Although $N_{\mathrm{ue}}$ is limited to 6, a large spatial diversity order of $N_{\mathrm{ue}} \times N_{\mathrm{mbs}}$ can be obtained for both downlink and uplink transmissions as $N_{\mathrm{mbs}}$ can be set arbitrary large. In the following, we will present the mathematical signal representations for OFDM downlink and SC uplink using STBC-TD.

#### 3.1.1 OFDM Downlink

Figure 3 illustrates the downlink transmitter/receiver structure. After STBC encoding, MRT-FDE is applied to obtain the transmit signal matrix of size $N_{\mathrm{mbs}} \times Q$, which is transmitted column by column in time by using $N_{\mathrm{mbs}}$ distributed antennas. Each UE is assigned a different set of $N_c/U$ subcarriers (e.g., the $u$th UE is assigned the subcarriers indexed as $k = u(N_c/U) \sim (u+1)(N_c/U) - 1$).

The matrix form expression $\mathbf{S}_{\downarrow_{\mathrm{stbc}}}(k)$ of size $N_{\mathrm{mbs}} \times Q$ for the downlink signals simultaneously transmitted from $N_{\mathrm{mbs}}$ distributed antennas is given as

$$\mathbf{S}_{\downarrow_{\mathrm{stbc}}}(k) = \sqrt{\frac{2E_s}{T_s}}\mathbf{W}_{\downarrow_{\mathrm{mrt}}}(k)\mathbf{X}(k), \tag{3}$$

where $\mathbf{W}_{\downarrow_{\mathrm{mrt}}}(k)$ is the $N_{\mathrm{mbs}} \times N_{\mathrm{ue}}$ MRT-FDE filter weight matrix. $E_s$ and $T_s$ denote data symbol energy and data symbol

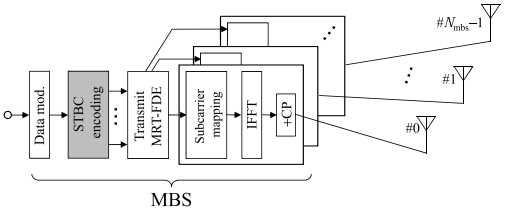


(a) Transmitter (MBS side)

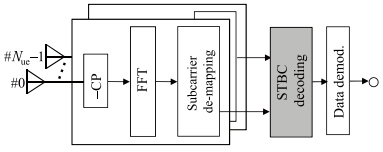


(b) Receiver (UE side)

**Fig. 3** STBC-TD for OFDM downlink transmission.

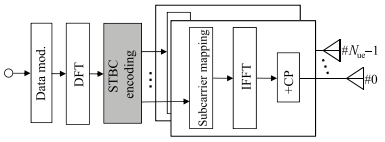


(a) Transmitter (UE side)

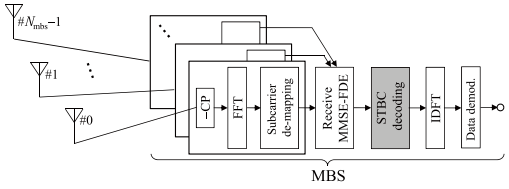


(b) Receiver (MBS side)

**Fig. 4** STBC-TD for SC uplink transmission.

duration, respectively. The $(n_{\rm mbs}, n_{\rm ue})$th element of $\mathbf{W}_{\downarrow_{\rm mrt}}(k)$ is derived as

$$W_{\downarrow_{\rm mrt}}(k; n_{\rm mbs}, n_{\rm ue}) = \frac{H^*_{\downarrow}(k; n_{\rm ue}, n_{\rm mbs})}{\sqrt{\frac{1}{N_c/U} \sum_{k=u(N_c/U)}^{(u+1)(N_c/U)-1} \sum_{n_{\rm mbs}=0}^{N_{\rm mbs}-1} \sum_{n_{\rm ue}=0}^{N_{\rm ue}-1} \left|H_{\downarrow}(k; n_{\rm ue}, n_{\rm mbs})\right|^2}}, \quad (4)$$

where $H_{\downarrow}(k; n_{\rm ue}, n_{\rm mbs})$ is the $(n_{\rm ue}, n_{\rm mbs})$th element of $\mathbf{H}_{\downarrow}(k)$.

The frequency-domain received signal matrix $\mathbf{R}(k)$ of size $N_{\rm ue} \times Q$ is expressed as

$$\mathbf{R}(k) = \mathbf{H}_{\downarrow}(k)\mathbf{S}_{\downarrow_{\rm stbc}}(k) + \mathbf{N}_{\downarrow}(k), \quad (5)$$

where $\mathbf{N}_{\downarrow}(k)$ is the $N_{\rm ue} \times Q$ equivalent noise (noise plus CCI) matrix. Each element of $\mathbf{N}_{\downarrow}(k)$ is independent zero-mean complex Gaussian variable with variance $2(N_0 + I_{0\downarrow}(u))/T_s$. STBC decoding to obtain the soft-decision symbols contains complex conjugation and addition/subtraction operations only [26], [28]. For Alamouti STBC ($J$=$Q$=2, $R_{\rm STBC}$=1), STBC decoding is expressed as

$$\begin{bmatrix} \hat{d}_0(k) \\ \hat{d}_1(k) \end{bmatrix} = \begin{bmatrix} R_{0,0}(k) + R^*_{1,1}(k) \\ R_{0,1}(k) - R^*_{1,0}(k) \end{bmatrix}, \quad (6)$$

where $R_{n_{\rm ue},q}(k)$ is the $(n_{\rm ue}, q)$th element of $\mathbf{R}(k)$.

### 3.1.2 SC Uplink

Figure 4 illustrates the uplink transmitter/receiver structure. Similar to the OFDM downlink transmission, $N_c/U$ subcarriers are exclusively assigned to the different UEs. Signals transmitted simultaneously from $N_{\rm ue}$ UE antennas are received by $N_{\rm mbs}$ distributed antennas.

The matrix form expression $\mathbf{S}_{\uparrow_{\rm stbc}}(k)$ of size $N_{\rm ue} \times Q$ for the uplink signals simultaneously transmitted from $N_{\rm ue}$ antennas is given as

$$\mathbf{S}_{\uparrow_{\rm stbc}}(k) = \sqrt{\frac{1}{N_{\rm ue}}\left(\frac{2E_s}{T_s}\right)}\mathbf{X}(k), \quad (7)$$

which is received by $N_{\rm mbs}$ distributed antennas. The received signal matrix $\mathbf{R}(k)$ of size $N_{\rm mbs} \times Q$ is given as

$$\mathbf{R}(k) = \mathbf{H}_{\uparrow}(k)\mathbf{S}_{\uparrow_{\rm stbc}}(k) + \mathbf{N}_{\uparrow}(k), \quad (8)$$

where $\mathbf{N}_{\uparrow}(k)$ is the $N_{\rm mbs} \times Q$ equivalent noise (noise plus CCI) matrix. Each element of $\mathbf{N}_{\uparrow}(k)$ is independent zero-mean complex Gaussian variable with variance $2(N_0 + I_{0\uparrow}(n_{\rm mbs}))/T_s$. After MMSE-FDE, we obtain

$$\hat{\mathbf{R}}(k) = \mathbf{W}_{\uparrow_{\rm mmse}}(k)\mathbf{R}(k), \quad (9)$$

where $\mathbf{W}_{\uparrow_{\rm mmse}}(k)$ is the MMSE-FDE filter weight matrix of size $N_{\rm ue} \times N_{\rm mbs}$ taking into account the CCI. The $(n_{\rm ue}, n_{\rm mbs})$th element of $\mathbf{W}_{\uparrow_{\rm mmse}}(k)$ in the presence of CCI is derived as

$$W_{\uparrow_{\rm mmse}}(k; n_{\rm ue}, n_{\rm mbs}) = \left(\sum_{n_{\rm ue}=0}^{N_{\rm ue}-1} \sum_{n_{\rm mbs}=0}^{N_{\rm mbs}-1} \frac{\left|H_{\uparrow}(k; n_{\rm mbs}, n_{\rm ue})\right|^2}{1 + \frac{I_{0\uparrow}(n_{\rm mbs})}{N_0}} + \left(\frac{1}{N_{\rm ue}}\frac{E_s}{N_0}\right)^{-1}\right)^{-1} \times \frac{H^*_{\uparrow}(k; n_{\rm mbs}, n_{\rm ue})}{1 + \frac{I_{0\uparrow}(n_{\rm mbs})}{N_0}}. \quad (10)$$

The same STBC decoding given by Eq. (6) is used to obtain the soft-decision symbols.

### 3.1.3 Link Capacity

OFDM downlink capacity $C_{\downarrow{\rm stbc},u}$ (bps/Hz) and SC uplink capacity $C_{\uparrow{\rm stbc},u}$ (bps/Hz) of the $u$th UE for the given UE locations is computed using Shannon capacity formula [30] as

$$\begin{cases} C_{\downarrow{\rm stbc},u} = \frac{1}{N_c/U} \sum_{k=u(N_c/U)}^{(u+1)(N_c/U)-1} \log_2\left(1 + \gamma_{\downarrow{\rm stbc},u}(k)\right). \\ C_{\uparrow{\rm stbc},u} = \log_2\left(1 + \gamma_{\uparrow{\rm stbc},u}\right). \end{cases} \quad (11)$$

In Eq. (11), $\gamma_{\downarrow{\rm stbc},u}(k)$ and $\gamma_{\uparrow{\rm stbc},u}$ denote the instantaneous SINR at the $k$th subcarrier after STBC decoding for OFDM downlink and that for SC uplink (note that for the SC uplink case, the instantaneous SINR is the same for all $N_c/U$ data symbols unlike the OFDM case). They are expressed as [11]

$$\begin{cases} \gamma_{\downarrow{\rm stbc},u}(k) = \frac{\frac{E_s}{N_0}\left|\hat{H}_{\downarrow}(k)\right|^2}{\mu^{\rm noise+CCI}_{\downarrow u}}. \\ \gamma_{\uparrow{\rm stbc},u} = \frac{\frac{1}{N_{\rm ue}}\frac{E_s}{N_0}\left|\frac{1}{N_c/U}\sum_{k=u(N_c/U)}^{(u+1)(N_c/U)-1}\hat{H}_{\uparrow}(k)\right|^2}{\mu^{\rm ISI}_{\uparrow u} + \mu^{\rm noise+CCI}_{\uparrow u}}. \end{cases} \quad (12)$$

where $\hat{H}_{\downarrow}(k)$ and $\hat{H}_{\uparrow}(k)$ are the equivalent channel gains of

$$\begin{cases} \mu_{\downarrow u}^{\text{noise+CCI}} = 1 + \frac{I_{0\downarrow}(u)}{N_0}. \\ \mu_{\uparrow u}^{\text{ISI}} = \frac{1}{N_{\text{ue}}} \frac{E_s}{N_0} \left\{ \frac{1}{N_c/U} \sum_{k=u(N_c/U)}^{(u+1)(N_c/U)-1} |\hat{H}_{\uparrow}(k)|^2 - \left| \frac{1}{N_c/U} \sum_{k=u(N_c/U)}^{(u+1)(N_c/U)-1} \hat{H}_{\uparrow}(k) \right|^2 \right\}. \\ \mu_{\uparrow u}^{\text{noise+CCI}} = \frac{1}{N_c/U} \sum_{k=u(N_c/U)}^{(u+1)(N_c/U)-1} \sum_{n_{\text{mbs}}=0}^{N_{\text{mbs}}-1} \left\{ \sum_{n_{\text{ue}}=0}^{N_{\text{ue}}-1} |W_{\downarrow\text{mmse}}(k; n_{\text{ue}}, n_{\text{mbs}})|^2 \times \left(1 + \frac{I_{0\uparrow}(n_{\text{mbs}})}{N_0}\right) \right\}. \end{cases} \tag{14}$$

downlink and uplink, respectively, and they are given as

$$\begin{cases} \hat{H}_{\downarrow}(k) = \dfrac{\sum_{n_{\text{ue}}=0}^{N_{\text{ue}}-1} \sum_{n_{\text{mbs}}=0}^{N_{\text{mbs}}-1} |H_{\downarrow}(k; n_{\text{ue}}, n_{\text{mbs}})|^2}{\sqrt{\frac{1}{N_c/U} \sum_{k=u(N_c/U)}^{(u+1)(N_c/U)-1} \sum_{n_{\text{ue}}=0}^{N_{\text{ue}}-1} \sum_{n_{\text{mbs}}=0}^{N_{\text{mbs}}-1} |H_{\downarrow}(k; n_{\text{ue}}, n_{\text{mbs}})|^2}}. \\ \hat{H}_{\uparrow}(k) = \sum_{n_{\text{ue}}=0}^{N_{\text{ue}}-1} \sum_{n_{\text{mbs}}=0}^{N_{\text{mbs}}-1} \dfrac{\frac{|H_{\uparrow}(k; n_{\text{mbs}}, n_{\text{ue}})|^2}{1+\frac{I_{0\uparrow}(n_{\text{mbs}})}{N_0}}}{\sum_{n_{\text{mbs}}=0}^{N_{\text{mbs}}-1} \sum_{n_{\text{ue}}=0}^{N_{\text{ue}}-1} \frac{|H_{\uparrow}(k; n_{\text{mbs}}, n_{\text{ue}})|^2}{1+\frac{I_{0\uparrow}(n_{\text{mbs}})}{N_0}} + \left(\frac{1}{N_{\text{ue}}} \frac{E_s}{N_0}\right)^{-1}}. \end{cases} \tag{13}$$

$\mu_{\downarrow u}^{\text{noise+CCI}}$, $\mu_{\uparrow u}^{\text{ISI}}$, and $\mu_{\uparrow u}^{\text{noise+CCI}}$ in Eq. (12) are the downlink noise plus CCI power, the uplink residual inter-symbol interference (ISI) power, and the uplink noise plus CCI power, respectively, which are given as Eq. (14)

### 3.2 MMSE-SVD for Multi-User Spatial Multiplexing

Multi-user spatial multiplexing of $U$ UEs is considered. $N_{\text{mbs}}(\geq U \cdot N_{\text{ue}})$ distributed antennas are selected from $N_{\text{macro}}$ distributed antennas to simultaneously transmit the $N_{\text{strm}}(\leq N_{\text{ue}})$ data streams per UE using $N_c$ subcarriers (the data stream is indexed by $n_{\text{strm}}$ (=0∼$N_{\text{strm}}$ − 1)). For multi-user spatial multiplexing in the OFDM downlink transmission, suppression of inter-user interference (IUI) and inter-antenna interference (IAI) is necessary. Whilst in the SC uplink transmission, suppression of ISI is necessary in addition to suppression of IAI and IUI.

For SC multi-user spatial multiplexing, frequency-domain maximum likelihood detection simultaneously suppressing the IUI, IAI, and ISI was proposed in [31]. The SVD based eigenmode transmission removing the IAI was proposed in [32]. Recently, a block diagonalization (BD) combined with SVD (BD-SVD) for downlink transmission was proposed [33]. BD-SVD applies BD to transform the multi-user channel into multiple single-user MIMO channels and then, applies SVD for eigenmode transmission of multiple data streams over each single-user MIMO channel. However, the spatial diversity gain will reduce since the spatial degree of freedom is used for BD [34]. Our proposed MMSE-SVD can avoid this problem by permitting IUI and IAI to remain to some extent (called the residual IUI and IAI).

#### 3.2.1 OFDM Downlink

Figure 5 illustrates the downlink transmitter/receiver structure. Assuming the eigenmode reception at each UE, the

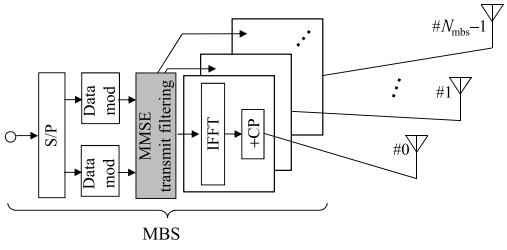


(a) Transmitter (MBS side)

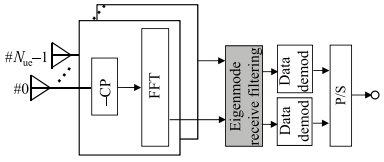


(b) Receiver (UE side)

**Fig. 5** MMSE-SVD for OFDM downlink transmission.

multi-user transmission using transmit MMSE filtering is carried out to suppress the IUI and IAI. The downlink signals transmitted from $N_{\text{mbs}}$ distributed antennas can be expressed in the matrix form as

$$\mathbf{S}_{\downarrow\text{mmse-svd}}(k) = \sqrt{\frac{2E_s}{T_s}} \mathbf{W}_{\downarrow\text{mmse}}(k) \begin{bmatrix} \mathbf{D}_{\downarrow 0}(k) \\ \vdots \\ \mathbf{D}_{\downarrow U-1}(k) \end{bmatrix}, \tag{15}$$

where $\mathbf{S}_{\downarrow\text{mmse-svd}}(k)$ is the $N_{\text{mbs}} \times 1$ vector and $\mathbf{D}_{\downarrow u}(k) = [d_{\downarrow u,0}(k), \ldots, d_{\downarrow u,n_{\text{strm}}}(k), \ldots, d_{\downarrow u,N_{\text{strm}}-1}(k)]^T$ is the $N_{\text{strm}} \times 1$ downlink transmit symbol vector of the $u$th UE. In the presence of CCI, the downlink transmit MMSE filter weight matrix $\mathbf{W}_{\downarrow\text{mmse}}(k)$ of size $N_{\text{mbs}} \times U \cdot N_{\text{strm}}$ is derived as

$$\begin{aligned} &\mathbf{W}_{\downarrow\text{mmse}}(k) \\ &= [\mathbf{W}_{\downarrow\text{mmse},0}(k), \ldots, \mathbf{W}_{\downarrow\text{mmse},u}(k), \ldots, \mathbf{W}_{\downarrow\text{mmse},U-1}(k)] \\ &= \left(\mathbf{U}_{\downarrow}^H(k)\mathbf{H}_{\downarrow}(k)\right)^H \\ &\quad \times \left( \begin{array}{l} \left(\mathbf{U}_{\downarrow}^H(k)\mathbf{H}_{\downarrow}(k)\right)\left(\mathbf{U}_{\downarrow}^H(k)\mathbf{H}_{\downarrow}(k)\right)^H \\ + \left(\frac{E_s}{N_0}\right)^{-1} \frac{N_{\text{ue}}}{U \cdot N_{\text{strm}}} \sum_{u=0}^{U-1} (1 + \frac{I_{0\downarrow}(u)}{N_0}) \mathbf{I}_{U \cdot N_{\text{strm}}} \end{array} \right)^{-1} \mathbf{P}_{\downarrow}^{1/2}(k), \end{aligned} \tag{16}$$

where $\mathbf{H}_{\downarrow}(k) = [\mathbf{H}_{\downarrow 0}^T(k), \ldots, \mathbf{H}_{\downarrow u}^T(k), \ldots, \mathbf{H}_{\downarrow U-1}^T(k)]^T$ is the downlink channel between $N_{\text{mbs}}$ distributed antennas and $U$ UE's antennas (each UE is equipped with $N_{\text{ue}}$ antennas). $\mathbf{U}_{\downarrow}(k) = diag[\mathbf{U}_{\downarrow 0}(k), \ldots, \mathbf{U}_{\downarrow u}(k), \ldots, \mathbf{U}_{\downarrow U-1}(k)]$, and $\mathbf{U}_{\downarrow u}(k)$ is obtained by applying SVD to the downlink channel $\mathbf{H}_{\downarrow u}(k)$ between $N_{\text{mbs}}$ distributed antennas and $N_{\text{ue}}$ antennas of the

$u$th UE as [35]

$$\mathbf{H}_{\downarrow u}(k) = \mathbf{U}_{\downarrow u}(k)\mathbf{\Lambda}_{\downarrow u}^{1/2}(k)\mathbf{V}_{\downarrow u}^{H}(k), \tag{17}$$

where $\mathbf{\Lambda}_{\downarrow u}(k)$ is the $N_{\text{strm}} \times N_{\text{strm}}$ diagonal matrix whose $n_{\text{strm}}$th diagonal element $\Lambda_{\downarrow u}(k; n_{\text{strm}})$ has the eigenvalue of the $n_{\text{strm}}$th eigenmode. In Eq. (16), $\mathbf{P}_{\downarrow}(k) = diag[\mathbf{P}_{\downarrow 0}(k), \ldots, \mathbf{P}_{\downarrow U-1}(k)]$ of size $U \cdot N_{\text{strm}} \times U \cdot N_{\text{strm}}$ represents the water-filling based power allocation [36] across eigenmodes and subcarriers. The $n_{\text{strm}}$th diagonal element of $\mathbf{P}_{\downarrow u}(k)$ is given as

$$P_{\downarrow u}(k; n_{\text{strm}}) = \left( \frac{1}{\lambda_{\downarrow u}} - \frac{1}{(\frac{E_s}{N_0})\Lambda_{\downarrow u}(k; n_{\text{strm}})} \right)^{+}, \tag{18}$$

$\lambda_{\downarrow u}$ is a constant which keeps the transmit power the unity, i.e.,

$$\frac{1}{N_{\text{strm}} \cdot N_c} \sum_{k=0}^{N_c-1} \sum_{n_{\text{strm}}=0}^{N_{\text{strm}}-1} P_{\downarrow u}(k; n_{\text{strm}}) \sum_{n_{\text{mbs}}=0}^{N_{\text{mbs}}-1} |A_u(k; n_{\text{mbs}}, n_{\text{strm}})|^2 = 1, \tag{19}$$

where $A_u(k; n_{\text{mbs}}, n_{\text{strm}})$ is the $(n_{\text{mbs}}, n_{\text{strm}})$th element of $\mathbf{W}_{\downarrow \text{mmse},u}(k)\mathbf{P}_{\downarrow}^{-1/2}(k)$ with $\mathbf{P}_{\downarrow}^{1/2}(k)\mathbf{P}_{\downarrow}^{-1/2}(k) = \mathbf{I}_{N_{\text{strm}}}$.

Denoting the $N_{\text{ue}} \times 1$ received signal vector at the $u$th UE by $\mathbf{R}_u(k)$ and the $N_{\text{strm}} \times N_{\text{ue}}$ eigenmode filter weight matrix by $\mathbf{W}_{\downarrow \text{svd},u}(k)$, the $N_{\text{strm}} \times 1$ soft-decision symbol vector $\hat{\mathbf{D}}_{\downarrow u}(k)$ is obtained by eigenmode reception as

$$\begin{aligned} \hat{\mathbf{D}}_{\downarrow u}(k) &= [\hat{d}_{\downarrow u,0}(k), \ldots, \hat{d}_{\downarrow u,n_{\text{strm}}}(k), \ldots, \hat{d}_{\downarrow u,N_{\text{strm}}-1}(k)]^T \\ &= \mathbf{W}_{\downarrow \text{svd},u}(k)\mathbf{R}_u(k) \end{aligned}, \tag{20}$$

where $\mathbf{R}_u(k)$ and $\mathbf{W}_{\downarrow \text{svd},u}(k)$ are given as

$$\begin{cases} \mathbf{R}_u(k) = \mathbf{H}_{\downarrow u}(k)\mathbf{S}_{\downarrow \text{mmse-svd}}(k) + \mathbf{N}_{\downarrow u}(k), \\ \mathbf{W}_{\downarrow \text{svd},u}(k) = \mathbf{U}_{\downarrow u}^{H}(k). \end{cases} \tag{21}$$

In Eq. (21), $\mathbf{N}_{\downarrow u}(k)$ is the $N_{\text{ue}} \times 1$ equivalent noise (noise plus CCI) vector. Each element of $\mathbf{N}_{\downarrow u}(k)$ is independent zero-mean complex Gaussian variable with variance $2(N_0 + I_{0\downarrow}(u))/T_s$.

### 3.2.2 SC Uplink

Figure 6 illustrates the uplink transmitter/receiver structure. Assuming the eigenmode transmission at each UE, the multi-user reception using MMSE receive filtering is carried out.

The uplink signals of $N_{\text{strm}}$ streams transmitted from the $u$th UE can be expressed in the matrix form as

$$\mathbf{S}_{\uparrow \text{mmse-svd},u}(k) = \sqrt{\frac{2E_s}{T_s}}\mathbf{W}_{\uparrow \text{svd},u}(k)\mathbf{D}_{\uparrow u}(k), \tag{22}$$

where $\mathbf{S}_{\uparrow \text{mmse-svd},u}(k)$ is the $N_{\text{ue}} \times 1$ vector, $\mathbf{D}_{\uparrow u}(k) = [d_{\uparrow u,0}(k), \ldots, d_{\uparrow u,n_{\text{strm}}}(k), \ldots, d_{\uparrow u,N_{\text{strm}}-1}(k)]^T$ is the $N_{\text{strm}} \times 1$ uplink transmit symbol vector of the $u$th UE, and $\mathbf{W}_{\uparrow \text{svd},u}(k)$ is the $N_{\text{ue}} \times N_{\text{strm}}$ uplink transmit MMSE filter weight matrix, which is given as

$$\mathbf{W}_{\uparrow \text{svd},u}(k) = \mathbf{V}_{\uparrow u}(k)\mathbf{P}_{\uparrow u}^{1/2}(k), \tag{23}$$

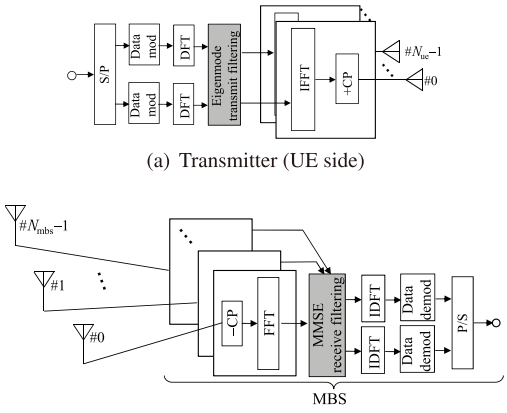


**Fig. 6** MMSE-SVD for SC ulink transmission.

where $\mathbf{V}_{\uparrow u}(k)$ is obtained by applying SVD to the uplink channel $\mathbf{H}_{\uparrow u}(k)$ between $N_{\text{ue}}$ antennas of the $u$th UE and $N_{\text{mbs}}$ distributed antennas, similarly to Eq. (17), as

$$\mathbf{H}_{\uparrow u}(k) = \mathbf{U}_{\uparrow u}(k)\mathbf{\Lambda}_{\uparrow u}^{1/2}(k)\mathbf{V}_{\uparrow u}^{H}(k), \tag{24}$$

where $\mathbf{\Lambda}_{\uparrow u}(k)$ is the $N_{\text{strm}} \times N_{\text{strm}}$ diagonal matrix whose $n_{\text{strm}}$th diagonal element $\Lambda_{\downarrow u}(k; n_{\text{strm}})$ has the eigenvalue of the $n_{\text{strm}}$th eigenmode. In Eq. (23), $\mathbf{P}_{\uparrow u}(k)$ of size $N_{\text{strm}} \times N_{\text{strm}}$ represents the MMSE power allocation across eigenmodes and subcarriers and its $n_{\text{strm}}$th diagonal element is given as

$$P_{\uparrow u}(k; n_{\text{strm}}) = \left( \frac{1}{\lambda_{\uparrow u}} \frac{1}{\sqrt{(\frac{E_s}{N_0})\Lambda_{\uparrow u}(k; n_{\text{strm}})}} - \frac{1}{(\frac{E_s}{N_0})\Lambda_{\uparrow u}(k; n_{\text{strm}})} \right)^{+}, \tag{25}$$

where $\lambda_{\uparrow u}$ is a constant which keeps the transmit power the unity, similarly to $\lambda_{\downarrow u}$. By using the above MMSE power allocation, ISI in SC uplink transmission can be suppressed.

Denoting the received signal vector at MBS by $\mathbf{R}(k)$ of size $N_{\text{mbs}} \times 1$ and the MMSE filter weight matrix by $\mathbf{W}_{\uparrow \text{mmse}}(k)$ of size $U \cdot N_{\text{strm}} \times N_{\text{mbs}}$, the soft-decision symbol vector $\hat{\mathbf{D}}_{\uparrow}(k)$ of $U \cdot N_{\text{strm}} \times 1$ is obtained by MMSE reception as

$$\begin{aligned} \hat{\mathbf{D}}_{\uparrow}(k) &= [\hat{\mathbf{D}}_{\uparrow 0}^{T}(k), \ldots, \hat{\mathbf{D}}_{\uparrow U-1}^{T}(k)]^T \\ &= \mathbf{W}_{\uparrow \text{mmse}}(k)\mathbf{R}(k) \end{aligned}, \tag{26}$$

with

$$\begin{aligned} \mathbf{R}(k) &= \sum_{u=0}^{U-1} \mathbf{H}_{\uparrow u}(k)\mathbf{S}_{\uparrow \text{mmse-svd},u}(k) + \mathbf{N}_{\uparrow u}(k) \\ &= \sqrt{\frac{2E_s}{T_s}}(\mathbf{H}_{\uparrow}(k)\mathbf{W}_{\uparrow \text{svd}}(k)) \begin{bmatrix} \mathbf{D}_{\uparrow 0}(k) \\ \vdots \\ \mathbf{D}_{\uparrow U-1}(k) \end{bmatrix} + \mathbf{N}_{\uparrow u}(k) \end{aligned}. \tag{27}$$

In the presence of CCI, $\mathbf{W}_{\uparrow \text{mmse}}(k)$ is derived as

$$\begin{aligned} \mathbf{W}_{\uparrow \text{mmse}}(k) &= (\mathbf{H}_{\uparrow}(k)\mathbf{W}_{\uparrow \text{svd}}(k))^H \\ &\times \begin{pmatrix} (\mathbf{H}_{\uparrow}(k)\mathbf{W}_{\uparrow \text{svd}}(k))(\mathbf{H}_{\uparrow}(k)\mathbf{W}_{\uparrow \text{svd}}(k))^H + (\frac{E_s}{N_0})^{-1} \\ \times diag\left(1 + \frac{I_{0\uparrow}(0)}{N_0}, \ldots, 1 + \frac{I_{0\uparrow}(N_{\text{mbs}}-1)}{N_0}\right) \end{pmatrix}^{-1}, \end{aligned} \tag{28}$$

where $\mathbf{H}_{\uparrow}(k) = [\mathbf{H}_{\uparrow 0}(k), \ldots, \mathbf{H}_{\uparrow u}(k), \ldots, \mathbf{H}_{\uparrow U-1}(k)]$ is the

uplink channel between $U$ UEs' antennas and $N_{\mathrm{mbs}}$ distributed antennas (each UE is equipped with $N_{\mathrm{ue}}$ antennas), $\mathbf{W}_{\uparrow\mathrm{svd}}(k) = diag[\mathbf{W}_{\uparrow\mathrm{svd},0}(k),\ldots,\mathbf{W}_{\uparrow\mathrm{svd},u}(k),\ldots,\mathbf{W}_{\uparrow\mathrm{svd},U-1}(k)]$, and $\mathbf{N}_{\uparrow}(k)$ is the $N_{\mathrm{mbs}} \times 1$ equivalent noise (noise plus CCI) vector. Each element of $\mathbf{N}_{\uparrow}(k)$ is independent zero-mean complex Gaussian variable with its $n_{\mathrm{mbs}}$th variance being given as $2(N_0 + I_{0\uparrow}(n_{\mathrm{mbs}}))/T_s$.

### 3.2.3 Link Capacity

The OFDM downlink capacity $C_{\downarrow\mathrm{mmse\text{-}svd},u}$ (bps/Hz) and the SC uplink capacity $C_{\uparrow\mathrm{mmse\text{-}svd},u}$ (bps/Hz) of the $u$th UE for the given UE locations is computed using

$$\begin{cases} C_{\downarrow\mathrm{mmse\text{-}svd},u} = \sum\limits_{n_{\mathrm{strm}}=0}^{N_{\mathrm{strm}}-1} \sum\limits_{k=0}^{N_c-1} \log_2\left(1+\gamma_{\downarrow\mathrm{mmse\text{-}svd},u}(k;n_{\mathrm{strm}})\right). \\ C_{\uparrow\mathrm{mmse\text{-}svd},u} = \sum\limits_{n_{\mathrm{strm}}=0}^{N_{\mathrm{strm}}-1} \log_2\left(1+\gamma_{\uparrow\mathrm{mmse\text{-}svd},u}(n_{\mathrm{strm}})\right). \end{cases} \tag{29}$$

In Eq. (29), $\gamma_{\downarrow\mathrm{mmse\text{-}svd},u}(k;n_{\mathrm{strm}})$ and $\gamma_{\uparrow\mathrm{mmse\text{-}svd},u}(n_{\mathrm{strm}})$ denote the instantaneous SINR at the $k$th subcarrier after eigenmode reception for OFDM downlink and the instantaneous SINR after MMSE reception for SC uplink. They are expressed as

$$\begin{cases} \gamma_{\downarrow\mathrm{mmse\text{-}svd},u}(k;n_{\mathrm{strm}}) = \dfrac{\frac{E_s}{N_0}\left|\hat{H}_{\downarrow u}(k;n_{\mathrm{strm}},u\cdot N_{\mathrm{strm}}+n_{\mathrm{strm}})\right|^2}{\mu_{\downarrow u}^{\mathrm{IAI}}(k;n_{\mathrm{strm}})+\mu_{\downarrow u}^{\mathrm{IUI}}(k;n_{\mathrm{strm}})+\mu_{\downarrow u}^{\mathrm{noise+CCI}}(k;n_{\mathrm{strm}})}, \\ \gamma_{\uparrow\mathrm{mmse\text{-}svd},u}(n_{\mathrm{strm}}) = \dfrac{\frac{E_s}{N_0}\left|\frac{1}{N_c}\sum\limits_{k=0}^{N_c-1}\hat{H}_{\uparrow u}(k;u\cdot N_{\mathrm{strm}}+n_{\mathrm{strm}},n_{\mathrm{strm}})\right|^2}{\mu_{\uparrow u}^{\mathrm{ISI}}(n_{\mathrm{strm}})+\mu_{\uparrow u}^{\mathrm{IAI}}(n_{\mathrm{strm}})+\mu_{\uparrow u}^{\mathrm{IUI}}(n_{\mathrm{strm}})+\mu_{\uparrow u}^{\mathrm{noise+CCI}}(n_{\mathrm{strm}})}, \end{cases} \tag{30}$$

where $\hat{H}_{\downarrow u}(k;n_{\mathrm{strm}},u\cdot N_{\mathrm{strm}}+n_{\mathrm{strm}})$ represents the equivalent downlink channel gain for the $u$th UE's $n_{\mathrm{strm}}$th stream and is the $(n_{\mathrm{strm}},u\cdot N_{\mathrm{strm}}+n_{\mathrm{strm}})$th element of $\hat{\mathbf{H}}_{\downarrow u}(k) = \mathbf{W}_{\downarrow\mathrm{svd},u}(k)\mathbf{H}_{\downarrow u}(k)\mathbf{W}_{\downarrow\mathrm{mmse}}(k)$ of size $N_{\mathrm{strm}} \times U\cdot N_{\mathrm{strm}}$ containing joint MMSE and SVD filtering. $\mu_{\downarrow u}^{\mathrm{IAI}}(k;n_{\mathrm{strm}})$, $\mu_{\downarrow u}^{\mathrm{IUI}}(k;n_{\mathrm{strm}})$, and $\mu_{\downarrow u}^{\mathrm{noise+CCI}}(k;n_{\mathrm{strm}})$ are respectively the residual IAI, residual IUI, and noise plus CCI corresponding to the $n_{\mathrm{strm}}$th stream of the $u$th UE, given by Eq. (31). $\hat{H}_{\uparrow u}(k;u\cdot N_{\mathrm{strm}}+n_{\mathrm{strm}},n_{\mathrm{strm}})$ is the equivalent uplink channel gain for the $u$th UE's $n_{\mathrm{strm}}$th stream, which is the $(u\cdot N_{\mathrm{strm}}+n_{\mathrm{strm}},n_{\mathrm{strm}})$th element of $\hat{\mathbf{H}}_{\uparrow u}(k) = \mathbf{W}_{\uparrow\mathrm{mmse}}(k)\mathbf{H}_{\uparrow u}(k)\mathbf{W}_{\uparrow\mathrm{svd},u}(k)$ of size $U\cdot N_{\mathrm{strm}} \times N_{\mathrm{strm}}$ containing joint MMSE and SVD filtering. $\mu_{\uparrow u}^{\mathrm{ISI}}(n_{\mathrm{strm}})$, $\mu_{\uparrow u}^{\mathrm{IAI}}(n_{\mathrm{strm}})$, $\mu_{\uparrow u}^{\mathrm{IUI}}(n_{\mathrm{strm}})$, and $\mu_{\uparrow u}^{\mathrm{noise+CCI}}(n_{\mathrm{strm}})$ are respectively the residual ISI, residual IAI, residual IUI, and noise plus CCI corresponding to the $n_{\mathrm{strm}}$th stream of the $u$th UE, given by Eq. (32). Here, $W_{\downarrow\mathrm{svd},u}(k;n_{\mathrm{strm}},n_{\mathrm{ue}})$ and $W_{\uparrow\mathrm{mmse}}(k;u\cdot N_{\mathrm{strm}}+n_{\mathrm{strm}},n_{\mathrm{mbs}})$ are respectively the $(n_{\mathrm{strm}},n_{\mathrm{ue}})$th element of $\mathbf{W}_{\downarrow\mathrm{svd},u}(k)$ of size $N_{\mathrm{strm}} \times N_{\mathrm{ue}}$ of the $u$th UE and the $(u\cdot N_{\mathrm{strm}}+n_{\mathrm{strm}},n_{\mathrm{mbs}})$th element of $\mathbf{W}_{\uparrow\mathrm{mmse}}(k)$ of size $U\cdot N_{\mathrm{strm}} \times N_{\mathrm{mbs}}$.

$$\begin{cases} \mu_{\downarrow u}^{\mathrm{IAI}}(k;n_{\mathrm{strm}}) = \left(\frac{E_s}{N_0}\right) \sum\limits_{\substack{n'_{\mathrm{strm}}=0, \\ n'_{\mathrm{strm}}\neq n_{\mathrm{strm}}}}^{N_{\mathrm{strm}}-1} \left|\hat{H}_{\downarrow u}(k;n_{\mathrm{strm}},u\cdot N_{\mathrm{strm}}+n'_{\mathrm{strm}})\right|^2. \\ \mu_{\downarrow u}^{\mathrm{IUI}}(k;n_{\mathrm{strm}}) = \\ \qquad \left(\frac{E_s}{N_0}\right) \sum\limits_{\substack{u'=0, \\ u'\neq u}}^{U-1} \sum\limits_{n_{\mathrm{strm}}=0}^{N_{\mathrm{strm}}-1} \left|\hat{H}_{\downarrow u}(k;n_{\mathrm{strm}},u'\cdot N_{\mathrm{strm}}+n_{\mathrm{strm}})\right|^2. \\ \mu_{\downarrow u}^{\mathrm{noise+CCI}}(k;n_{\mathrm{strm}}) = \left(1+\frac{I_{0\downarrow}(u)}{N_0}\right) \sum\limits_{n_{\mathrm{ue}}=0}^{N_{\mathrm{ue}}-1} \left|W_{\downarrow\mathrm{svd},u}(k;n_{\mathrm{strm}},n_{\mathrm{ue}})\right|^2. \end{cases} \tag{31}$$

## 3.3 Blind SLM for SC uplink using STBC-TD

When using CDAT, the PAPR of SC uplink signal increases. The reason for PAPR increase of SC transmit signal when using STBC-TD and MMSE-SVD is given below. The SC signal considered in this paper is an ideal rectangular-filtered SC signal, which is equivalent to DFT-precoded OFDM signal. The ideal rectangular filter generates the impulse response with large sidelobe amplitudes and long lasting in time-domain and consequently, increases the PAPR [37]. Although STBC-TD keeps the same PAPR as single-antenna transmission, MMSE-SVD further increases the PAPR because of additional MMSE transmit filtering. Therefore, PAPR reduction technique is still needed when CDAT is used. To reduce the PAPR, SLM can be carried out by multiplying a phase rotation sequence to the transmit SC signal in either time-domain or frequency-domain [16]. Blind SLM without requiring the transmission of side information (phase rotation sequence information) is described in the following.

The SC uplink transmission using STBC-TD of coding parameters ($J$, $Q$, and $R_{\mathrm{STBC}}$) is considered. Assuming STBC code like Alamouti code of Eq. (2), any block in $J$ blocks appears only once among $Q$ blocks, hence SLM can be applied before STBC encoding. If PAPR is computed after STBC encoding, the number of PAPR computations per code word can be reduced by about $N_{\mathrm{ue}}/R_{\mathrm{STBC}}$ times from $M \times N_{\mathrm{ue}} \times Q$ to $M \times J$ times, where $M$ and $N_{\mathrm{ue}}$ denote the number of phase rotation sequence candidates and the number of UE antennas, respectively.

Both frequency-domain SLM (FD-SLM) and time-domain SLM (TD-SLM) are considered. At the receiver side, de-mapping is done to remove the phase rotation applied to the transmit signal. Since no side information is transmitted, it is necessary to estimate which phase rotation sequence is multiplied to the transmit signal. Incorrect sequence selection significantly distorts the received signal constellation after de-mapping. Blind SLM exploits this fact. For signal detection, a phase rotation sequence candidate is selected which provides the minimum squared error between the received signal after de-mapping and original constellation.

Transmitter/receiver structure of SC uplink using STBC-TD and blind FD-SLM is illustrated in Fig. 7. If blind TD-SLM is used, phase rotation sequence selection is done in the time-domain before discrete Fourier transform (DFT).

$$\begin{cases} \mu_{\uparrow u}^{\mathrm{ISI}}(n_{\mathrm{strm}}) = (\frac{E_s}{N_0})\left(\frac{1}{N_c}\sum_{k=0}^{N_c-1}\left|\hat{H}_{\uparrow u}(k; u\cdot N_{\mathrm{strm}}+n_{\mathrm{strm}}, n_{\mathrm{strm}})\right|^2 - \left|\frac{1}{N_c}\sum_{k=0}^{N_c-1}\hat{H}_{\uparrow u}(k; u\cdot N_{\mathrm{strm}}+n_{\mathrm{strm}}, n_{\mathrm{strm}})\right|^2\right). \\ \mu_{\uparrow u}^{\mathrm{IAI}}(n_{\mathrm{strm}}) = (\frac{E_s}{N_0})\frac{1}{N_c}\sum_{k=0}^{N_c-1}\left(\sum_{\substack{n'_{\mathrm{strm}}=0,\\ n'_{\mathrm{strm}}\neq n_{\mathrm{strm}}}}^{N_{\mathrm{strm}}-1}\left|\hat{H}_{\uparrow u}(k; u\cdot N_{\mathrm{strm}}+n_{\mathrm{strm}}, n'_{\mathrm{strm}})\right|^2\right). \\ \mu_{\uparrow u}^{\mathrm{IUI}}(n_{\mathrm{strm}}) = (\frac{E_s}{N_0})\frac{1}{N_c}\sum_{k=0}^{N_c-1}\left(\sum_{\substack{u'=0,\\ u'\neq u}}^{U-1}\sum_{n_{\mathrm{strm}}=0}^{N_{\mathrm{strm}}-1}\left|\hat{H}_{\uparrow u'}(k; u\cdot N_{\mathrm{strm}}+n_{\mathrm{strm}}, n_{\mathrm{strm}})\right|^2\right). \\ \mu_{\uparrow u}^{\mathrm{noise+CCI}}(n_{\mathrm{strm}}) = \frac{1}{N_c}\sum_{k=0}^{N_c-1}\sum_{n_{\mathrm{mbs}}=0}^{N_{\mathrm{mbs}}-1}\left(1+\left|W_{\uparrow\mathrm{mmse}}(k; u\cdot N_{\mathrm{strm}}+n_{\mathrm{strm}}, n_{\mathrm{mbs}})\right|^2\frac{I_{0\uparrow}(n_{\mathrm{mbs}})}{N_0}\right). \end{cases} \tag{32}$$

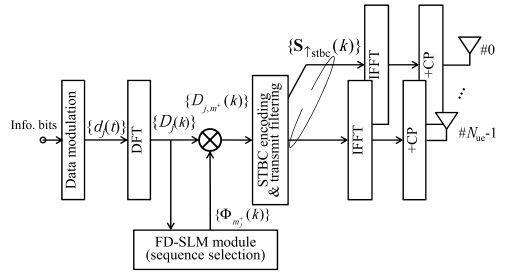


(a) Transmitter

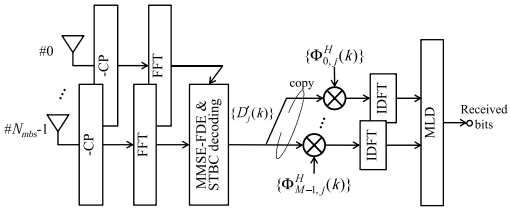


(b) Receiver

**Fig. 7** Blind FD-SLM.

Without loss of generality, we omit the UE index $u$ in the following.

### 3.3.1 Blind FD-SLM

The $j$th block data symbol sequence $\{d_j(t); t = 0 \sim N_c/U - 1\}$ is transformed by $N_c/U$ point DFT into the frequency-domain signal $\{D_j(k); k = 0 \sim N_c/U - 1\}$. Then, the $m$th phase rotation sequence $\{\Phi_m(k); k = 0 \sim N_c/U - 1\}$ is multiplied to obtain $\{D_{j,m}(k); k = 0 \sim N_c/U - 1\}$ for $m = 0 \sim M - 1$. After applying $V \cdot N_c$ point inverse fast Fourier transform (IFFT), the PAPR of the time-domain signal $\{d_{j,m}(t); t = 0 \sim V \cdot N_c - 1\}$ is computed, where $V$ is the over-sampling ratio. The selection of phase rotation sequence is carried out according to the following two selection criteria.

- Mini-max: the same phase rotation sequence is applied to all $J$ data blocks. The rotation sequence that minimizes the maximum PAPR among $J$ data blocks before STBC encoding is selected.
- Block-by-block minimization: the different phase rotation sequences are applied to different data blocks. For each of $J$ data blocks, one phase sequence that minimizes the PAPR before STBC encoding is selected.

The above sequence selection criteria can be expressed as

$$\begin{cases} m^{\doteq} = \arg\min_{m=0\sim M-1}\left\{\max_{j=0\sim J-1}\mathrm{PAPR}(d_{j,m}(t))\right\} \\ \qquad\qquad \text{for mini-max,} \\ m_j^{\doteq} = \arg\min_{m=0\sim M-1}\left\{\mathrm{PAPR}(d_{j,m}(t))\right\} \\ \qquad\qquad \text{for block-by-block min.,} \end{cases} \tag{33}$$

where

$$\mathrm{PAPR}(\{d_{j,m}(t)\}) = \frac{\max\{|d_{j,m}(t)|^2; t = 0, 1, \ldots, V\cdot N_c - 1\}}{\frac{1}{VN_c}\sum_{t=0}^{V\cdot N_c-1}|d_{j,m}(t)|^2}, \tag{34}$$

with

$$d_{j,m}(t) = \begin{cases} \frac{1}{\sqrt{V\cdot N_c}}\sum_{k=0}^{N_c-1}\Phi_m(k)D_j(k)\exp\left(i2\pi t\frac{k}{V\cdot N_c}\right) \\ \qquad\qquad \text{for mini-max,} \\ \frac{1}{\sqrt{V\cdot N_c}}\sum_{k=0}^{N_c-1}\Phi_{m,j}(k)D_j(k)\exp\left(i2\pi t\frac{k}{V\cdot N_c}\right) \\ \qquad\qquad \text{for block-by-block min.,} \end{cases} \tag{35}$$

where $i = \sqrt{-1}$. After multiplying the phase rotation sequence, STBC encoding is applied to generate the uplink transmit signal as in Eq. (7).

The uplink transmit signal is received by $N_{\mathrm{mbs}}$ distributed antennas for MMSE-FDE and STBC decoding (which are respectively expressed by Eqs. (8) and (6)) to obtain the frequency-domain received signal $\{D'_j(k); k = 0 \sim N_c/U - 1\}$. In the case of blind FD-SLM, the complex conjugate of $m$th phase rotation sequence candidate $\{\Phi_m(k); k = 0 \sim N_c/U - 1\}$ is multiplied and then, brought back by $N_c/U$ point IDFT to the time-domain signal $\{d'_{j,m}(t); t = 0 \sim N_c/U - 1\}$. Then, the squared error between the received signal after de-mapping and original constellation is computed. This is done for all phase rotation sequence candidates to search for the candidate having the minimum squared error.

The soft-decision symbol sequence $\{d'_j(t); t = 0 \sim N_c/U-1\}$ after de-mapping is expressed as

$$\begin{cases} \hat{d}_j(t) = \frac{1}{\sqrt{N_c/U}} \sum_{k=0}^{N_c/U-1} D'_j(k)\Phi^*_{\hat{m}}(k) \exp\left(i2\pi t \frac{k}{N_c/U}\right), \\ \hat{m} = \arg \min_{\substack{m=0\sim M-1, \\ d(t)\in D}} \sum_{t=0}^{N_c/U-1} \left|d(t) - d'_{j,m}(t)\right|^2, \end{cases} \tag{36}$$

where $d(t)$ denotes the data symbol candidate at symbol time $t$ in the signal constellation set $D$.

### 3.3.2 Blind TD-SLM

Similar to blind FD-SLM, mini-max and block-by-block min. criteria can be used for the phase rotation sequence selection. The difference of blind TD-SLM from blind FD-SLM is only the use of time-domain phase rotation sequence candidates. Hence, description of the phase rotation sequence selection at the transmitter and the de-mapping at the receiver is omitted for the sake of brevity.

## 4. Monte-Carlo Computer Simulation

### 4.1 Simulation Setting

A simple hexagonal cellular model with $N_{\text{macro}}$=7 distributed antennas located uniformly in each macro-cell is assumed, as shown in Fig. 8. For comparison purpose, a macro-cell network with 7 co-located antennas/MBS is also shown in the figure. Simulation parameters are summarized in Table 2. The macro-cell of interest is surrounded by 6 adjacent macro-cells. In each macro-cell, $U$=2 UEs having $N_{\text{ue}}$=2 antennas are randomly located. The number of data streams per UE is assumed to be $N_{\text{strm}}$=2 for MMSE-SVD. $N_{\text{mbs}}$=4 distributed antennas are selected from $N_{\text{macro}}$=7 distributed antennas in a descending order of the instantaneous received signal power level for up/downlink transmissions (TDD is assumed). In the case of STBC-TD, the sum of instantaneous path gains between each distributed antenna and $N_{\text{ue}}$=2 UE antennas is computed and then, $N_{\text{mbs}}$=4 distributed antennas are selected from $N_{\text{macro}}$=7 distributed antennas for each UE in a descending order of the sum of instantaneous path gains. On the other hand, in the case of MMSE-SVD, the instantaneous path gain between each distributed antenna and each UE antenna is computed and then, $N_{\text{mbs}}$=4 distributed antennas are selected for each UE antenna in a descending order of instantaneous path gains.

The total number of subcarriers is $N_c$=128. Multi-access scheme for STBC-TD is FDMA. 128 subcarriers are divided to 2 subcarrier-blocks, each block is assigned to one of 2 UEs. On the other hand, all 128 subcarriers are shared by 2 UEs for MMSE-SVD. Frequency-selective fading channel having 16-path uniform power delay profile (PDP) is assumed as well as shadowing loss and path loss. It is assumed that the channel becomes Nakagami-Rice channel with $K$=10 dB when the distance between distributed antenna and UE is shorter than $R'=R/\sqrt{7}$, otherwise

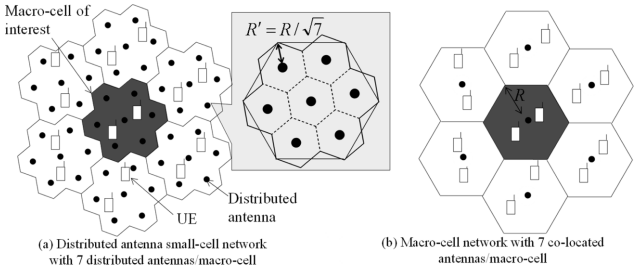


**Fig. 8** Cellular model.

**Table 2** Simulation parameters.

| | | | |
|---|---|---|---|
| Tx/Rx | SC uplink | FDMA | STBC-TD w/ Rx-FDE |
| | | Multi-user spatial multiplexing | MMSE-SVD |
| | OFDM downlink | FDMA | STBC-TD w/ Tx-FDE |
| | | Multi-user spatial multiplexing | MMSE-SVD |
| | Total no. of subcarriers | | $N_c$=128 |
| | GI length | | $N_g$=32 |
| | No. of distributed antennas deployed in a macro-cell | | $N_{\text{macro}}$=7 |
| | No. of UE antennas | | $N_{\text{ue}}$=2 |
| | No. of distributed antennas to be selected | | $N_{\text{mbs}}$=4 |
| | Channel state information | | Ideal |
| Propag. channel | Path loss exponent | | $\alpha$=3.5 |
| | Shadowing loss standard deviation | | $\sigma$=7.0(dB) |
| | Type of fading | | Frequency-selective block Nakagami-Rice and Rayleigh |
| | $K$-factor of Nakagami-Rice | | $K$=10dB |
| | Power-delay profile shape | | $L$=16 - uniform |

the channel becomes Rayleigh channel, where $R$ denotes the macro-cell radius. The root-mean square (rms) delay spread is an important factor which affects the transmission performance. If a subcarrier separation of 240 kHz is assumed (i.e., the transmission bandwidth becomes 30.72 MHz), the OFDM symbol length becomes 4.17 $\mu$s, one sample time length becomes 32.6 ns and hence, the rms delay spread becomes 150 ns and 83.8 ns for Rayleigh fading and Nakagami-Rice fading with $K$=10, respectively.

Assuming interference-limited condition, the distributions of uplink/downlink capacities are obtained by Monte-Carlo computer simulation. The knowledge of CCI from adjacent macro-cells is necessary for computing the receive MMSE-FDE filter weight matrix for SC uplink using STBC-TD and for computing the MMSE filter weight matrices for OFDM downlink/SC uplink using MMSE-SVD. Perfect knowledge of CCI is assumed in the paper.

The downlink channel gain at the $k$th subcarrier between the $u$th UE of the macro-cell of interest and the $n_{\text{mbs}}$th distributed antenna of the $c$(=1∼6)th adjacent macro-cell is denoted by $H_{\downarrow u}(k; n_{\text{ue}}, n_{\text{mbs}}(c))$. The uplink channel gain at the $k$th subcarrier between the $n_{\text{ue}}$th antenna of the $u$th UE of the $c$(=1∼6)th adjacent macro-cell and the $n_{\text{mbs}}$th distributed antenna of the macro-cell of interest is denoted by

$$\begin{cases} \dfrac{I_{0\downarrow}(u)}{N_0} = \left(\dfrac{E_s}{N_0}\right) \displaystyle\sum_{c=1}^{6} \sum_{n_{\mathrm{mbs}}(c)=0}^{N_{\mathrm{mbs}}-1} \sum_{n_{\mathrm{ue}}(c)=0}^{N_{\mathrm{ue}}-1} E\left[\left|W_{\downarrow\mathrm{mrt}}(k; n_{\mathrm{mbs}}(c), n_{\mathrm{ue}}(c)) H_{\downarrow}(k; n_{\mathrm{ue}}, n_{\mathrm{mbs}}(c))\right|^2\right] \\ \qquad = \dfrac{1}{N_{\mathrm{mbs}}} \left(\dfrac{E_s}{N_0}\right) \displaystyle\sum_{c=1}^{6} \sum_{n_{\mathrm{mbs}}(c)=0}^{N_{\mathrm{mbs}}-1} \left(d_{u,n_{\mathrm{mbs}}(c)}^{-\alpha} \cdot 10^{-\eta_{u,n_{\mathrm{mbs}}(c)}/10}\right) \\ \dfrac{I_{0\uparrow}(n_{\mathrm{mbs}})}{N_0} = \dfrac{1}{N_{\mathrm{ue}}} \left(\dfrac{E_s}{N_0}\right) \displaystyle\sum_{c=1}^{6} \dfrac{1}{N_c/U} \times \sum_{k=u(N_c/U)}^{(u+1)(N_c/U)-1} \sum_{n_{\mathrm{ue}}(c)=0}^{N_{\mathrm{ue}}-1} E\left[\left|H_{\uparrow}(k; n_{\mathrm{mbs}}, n_{\mathrm{ue}}(c))\right|^2\right] \\ \qquad = \left(\dfrac{E_s}{N_0}\right) \displaystyle\sum_{c=1}^{6} \left(d_{u(c),n_{\mathrm{mbs}}}^{-\alpha} \cdot 10^{-\eta_{u(c),n_{\mathrm{mbs}}}/10}\right) \end{cases} \quad \text{for STBC-TD,} \tag{37}$$

$$\begin{cases} \dfrac{I_{0\downarrow}(u)}{N_0} = \left(\dfrac{E_s}{N_0}\right) \displaystyle\sum_{c=1}^{6} \sum_{u(c)=0}^{U-1} \sum_{n_{\mathrm{strm}}=0}^{N_{\mathrm{strm}}-1} \sum_{n_{\mathrm{mbs}}(c)=0}^{N_{\mathrm{mbs}}-1} E\left[\left|H_{\downarrow} u(k; n_{\mathrm{ue}}, n_{\mathrm{mbs}}(c)) W_{\downarrow\mathrm{mmse}}(k; n_{\mathrm{mbs}}(c), u(c) \cdot N_{\mathrm{strm}} + n_{\mathrm{strm}})\right|^2\right] \\ \qquad = \left(\dfrac{E_s}{N_0}\right) \displaystyle\sum_{c=1}^{6} \sum_{n_{\mathrm{mbs}}(c)=0}^{N_{\mathrm{mbs}}-1} \left(d_{u,n_{\mathrm{mbs}}(c)}^{-\alpha} \cdot 10^{-\eta_{u,n_{\mathrm{mbs}}(c)}/10}\right) \\ \dfrac{I_{0\uparrow}(n_{\mathrm{mbs}})}{N_0} = \left(\dfrac{E_s}{N_0}\right) \displaystyle\sum_{c=1}^{6} \sum_{u(c)=0}^{U-1} \sum_{n_{\mathrm{strm}}=0}^{N_{\mathrm{strm}}-1} \dfrac{1}{N_c} \sum_{k=0}^{N_c-1} \sum_{n_{\mathrm{ue}}(c)=0}^{N_{\mathrm{ue}}-1} E\left[\left|H_{\uparrow} u(k; n_{\mathrm{mbs}}, n_{\mathrm{ue}}(c)) W_{\uparrow\mathrm{svd}}(k; n_{\mathrm{ue}}(c), n_{\mathrm{strm}})\right|^2\right] \\ \qquad = N_{\mathrm{ue}} \left(\dfrac{E_s}{N_0}\right) \displaystyle\sum_{c=1}^{6} \sum_{u(c)=0}^{U-1} \left(d_{u(c),n_{\mathrm{mbs}}}^{-\alpha} \cdot 10^{-\eta_{u(c),n_{\mathrm{mbs}}}/10}\right) \end{cases} \quad \text{for MMSE-SVD,} \tag{38}$$

$H_{\uparrow u}(k; n_{\mathrm{mbs}}, n_{\mathrm{ue}}(c))$.

The downlink and uplink CCI power spectrum densities, $I_{0\downarrow}(u)$ and $I_{0\uparrow}(n_{\mathrm{mbs}})$, are computed using Eqs. (37) and (38) for STBC-TD and MMSE-SVD, respectively, where $d_{u,n_{\mathrm{mbs}}(c)}^{-\alpha}$ and $10^{-\eta_{u,n_{\mathrm{mbs}}(c)}/10}$ are respectively the distance and the shadowing loss of the propagation channel between the $u$th UE of the macro-cell of interest and the $n_{\mathrm{mbs}}(c)$th distributed antenna of the $c$th adjacent macro-cell. $d_{u(c),n_{\mathrm{mbs}}}^{-\alpha}$ and $10^{-\eta_{u(c),n_{\mathrm{mbs}}}/10}$ are respectively the distance and the shadowing loss of the propagation channel between the $u(c)$th UE of the $c$th adjacent macro-cell and the $n_{\mathrm{mbs}}$th distributed antenna of the macro-cell of interest.

### 4.2 STBC-TD and MMSE-SVD

The capacity distribution obtained by computer simulation is plotted in Fig. 9. For the comparison, single-input single-output (SISO) case in a macro-cell network is plotted. The use of 7 co-located antennas improves the link capacity of the macro-cell network. It is clearly shown that further improvement in the link capacity is achieved by distributing 7 antennas over a macro-cell area. CCI from 7 adjacent macro-cells are taken into account to compute the uplink MMSE filter weight matrix given by Eq. (10) for STBC-TD and the downlink/uplink MMSE filter weight matrices given by Eqs. (16) and (28) for MMSE-SVD. Note that MRT-FDE filter weight matrix is used for downlink of STBC-TD and hence, CCI does not need to take into account. Comparison between STBC-TD and MMSE-SVD shows that MMSE-SVD lowers the outage probability at higher link capacity region (e.g., around 5 bps/Hz) while STBC-TD lowers the outage probability at lower link capacity region (e.g., around 1 bps/Hz). The possible reason for the above is discussed below. MMSE-SVD is used for spatial division multiaccess (SDMA) while STBC-TD assumes FDMA. Note that the bandwidth per UE reduces by a factor $U$ of the number of UEs for STBC-TD while it remains the same for MMSE-SVD. Therefore, MMSE-SVD is capable of achieving higher link capacity than STBC-TD in a good propagation environment. However, in a poor propagation environment such as near the macro-cell edge, The impact of the residual IUI becomes significantly large for MMSE-SVD. Furthermore, STBC-TD achieves full spatial diversity gain while MMSE-SVD cannot (see Sect. 3.2). Therefore, STBC-TD provides lower outage probability than MMSE-SVD.

Downlink capacity comparison between MMSE-SVD with and without taking into account CCI (w/ and w/o CCI info in the figure) and BD-SVD [33] is shown in Fig. 10. It can be seen from the figure that in multi-macro-cell environment, although MMSE-SVD w/o taking into account the CCI provides lower capacity than BD-SVD, it provides higher capacity if the CCI is taken into account.

The impact of imperfect CSI on the 50% outage sum link capacity of downlink for STBC-TD and MMSE-SVD under a single-cell environment (i.e., without CCI) is plotted in Fig. 11 assuming $N_{\mathrm{mbs}}$=4, $U$=2, and $N_{\mathrm{ue}}$=2. The CSI error is modeled as a Gaussian variable and the time-varying fading induced CSI error is also considered. The CSI error factor $\varepsilon$ is introduced, which is defined by the rms CSI error normalized by the rms value of AWGN. The normalized maximum Doppler frequency $f_D\tau$ is introduced to represent the severity of time-varying fading, where $\tau$ is the time difference between time when CSI is obtained and time when it is used to construct the transmit filter. It is clearly seen from Fig. 11 that the sum link capacity achievable with MMSE-SVD degrades as either $\varepsilon$ or $f_D\tau$ increases. The sum link capacity is quite sensitive to $f_D\tau$ and it degrades by about 30% when $f_D\tau$=0.1 (which corresponds to the UE speed of 108 km/h assuming 5 GHz carrier frequency and $\tau$=0.2 ms).

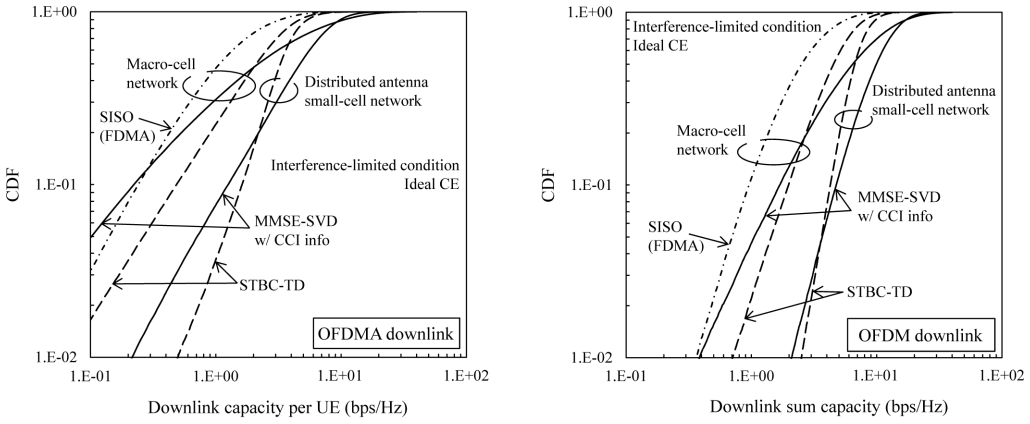


(a) OFDM downlink

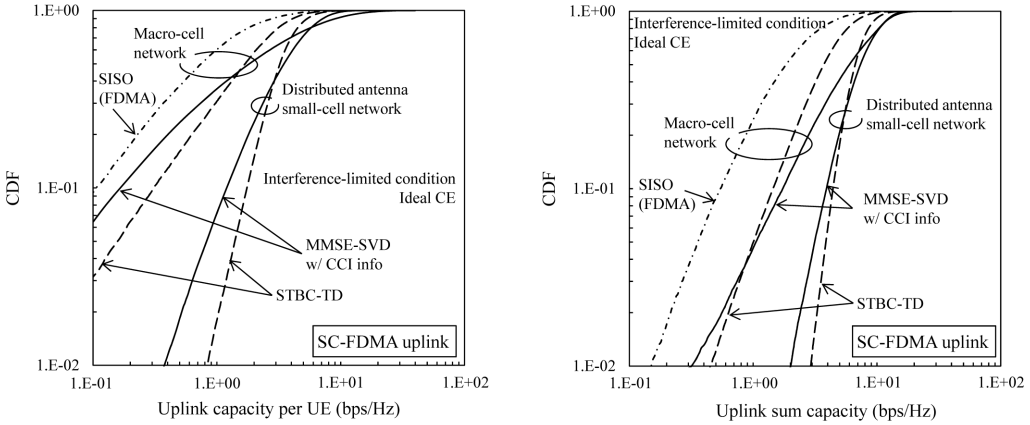


(b) SC uplink

**Fig. 9** Link capacity distribution.

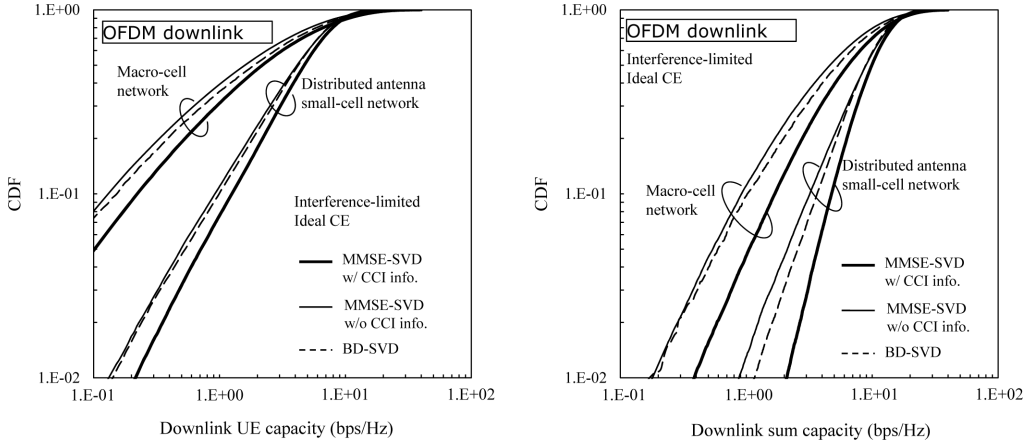


**Fig. 10** Comparison between MMSE-SVD and BD-SVD.

On the other hand, the CSI error has less impact on the sum link capacity achievable with STBC-TD. It can be seen from Fig. 11 that, although the capacity remains almost unchanged as $\varepsilon$ increases, it drops by about 20% when $f_D\tau$=0.3 (which corresponds to the UE speed of 324 km/h assuming 5 GHz carrier frequency and $\tau$=0.2 ms).

### 4.3 Blind SLM

How blind SLM reduces the PAPR of SC signal with STBC-TD is plotted in Fig. 12. The uplink SC signal using 64 subcarriers and 16 QAM data modulation is considered. STBC parameters are set to $(J,Q,R_{\mathrm{STBC}})$=(2,2,1) when the number

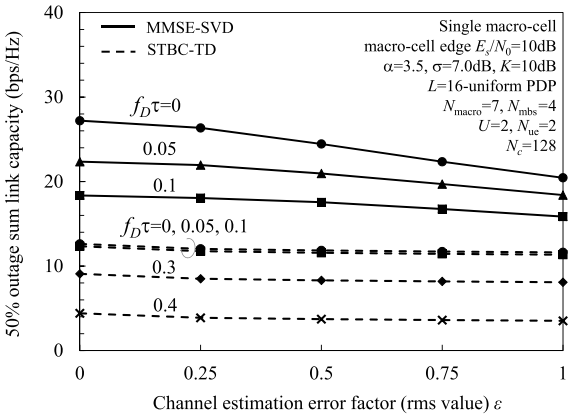


**Fig. 11** Impact of CSI error on 50% outage sum link capacity.

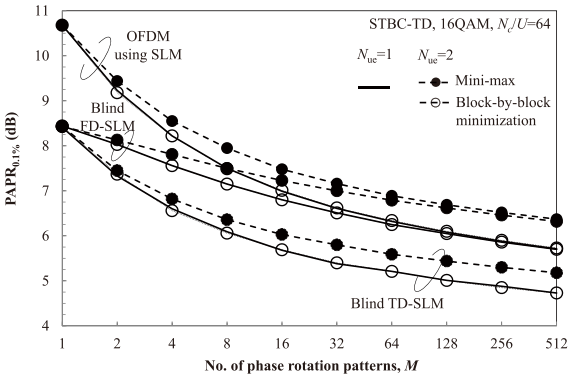


**Fig. 12** PAPR of uplink SC signal with STBC-TD.

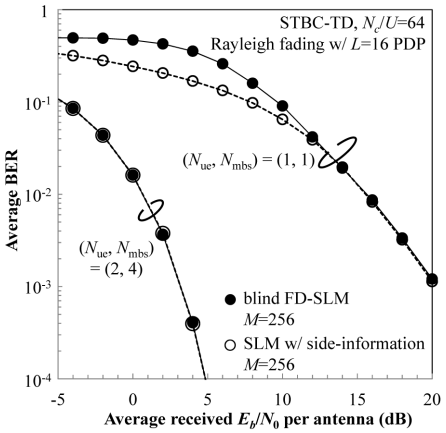


(a) Blind FD-SLM

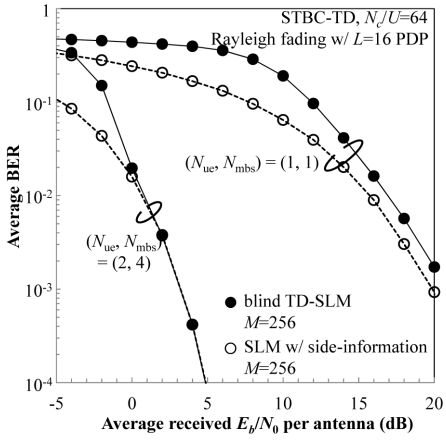


(b) Blind TD-SLM

**Fig. 13** BER performance of SC signal transmission with STBC-TD and blind SLM.

of UE antennas is $N_{ue}$=2. Each element of the phase rotation sequence candidates is randomly chosen from 3 phases, i.e., (0, 2π/3, 4π/3) radians. Fig. 12 shows that increasing the number $M$ of phase rotation sequences can further reduce the PAPR. TD-SLM can reduce the PAPR more effectively than FD-SLM for the same value of $M$. This is because the resulting samples of phase-rotated signals obtained from TD-SLM are in a bounded set (i.e., 16×3=48 patterns when assuming 16QAM and polyphase rotations of (0, 2π/3, 4π/3) radians), while the signal constellation after applying the phase rotation according to FD-SLM widely scatters. This causes the phase-rotated signal from TD-SLM becomes closer to optimal solution than FD-SLM at the same $M$ [38]. Blind TD-SLM using block-by-block minimization criterion provides the lowest PAPR in the cases of $N_{ue}$=2. Blind TD-SLM with $M$=256 can reduce the PAPR of SC signal by 3.6 dB; the PAPR is 1 dB lower than that of OFDM.

The uncoded average bit error rate (BER) performance of blind SLM is plotted in Fig. 13. For comparison, the BER performances with side information (the perfect knowledge of phase rotation sequence index) are also plotted. Although blind TD-SLM provides slightly degraded BER performance than TD-SLM with side information when $N_{ue}$=1 (no STBC-TD), blind TD-SLM achieves BER performance close to TD-SLM with side information when STBC-TD is used. The reason for this is discussed below. The frequency-selective fading produces ISI. The receive MMSE-FDE cannot remove the ISI unlike the receive zero-forcing type FDE (ZF-FDE) and hence, the ISI remains to some extent (this is called the residual ISI). However, a combined use of MMSE-FDE and STBC-TD can significantly reduce the residual ISI owing to the spatial diversity gain and consequently, the accuracy of phase rotation sequence estimation is improved. Accordingly, blind TD-SLM achieves BER performance close to TD-SLM with side information.

Meanwhile, it is seen that the BER degrades when $E_b/N_0$ is low even when $N_{ue}$=2. The reason of this degradation can be described as follows. The phase rotation sequence estimation and data detection in blind SLM (both TD-SLM and FD-SLM) utilizes a fact that the received signal constellation observed after correct de-mapping (i.e., the phase rotation due to SLM is perfectly removed) and that observed after incorrect de-mapping are quite different. Therefore, the phase rotation sequence that has been used at the transmitter side can be estimated by using maximum likelihood (ML) estimation [17], [18]. However, this is only true when the received SNR is sufficiently high. In a low

SNR region, due to the noise, the differentiation between correct de-mapping and incorrect de-mapping becomes ambiguous and an erroneous estimation of phase rotation sequence happens. As a consequence, the BER tends to degrade in a low SNR region.

## 5. Conclusion

Key to realizing 5G networks is advanced utilization of spatial-domain. In this paper, we presented the recent advances in cooperative distributed antenna transmission (CDAT) techniques. Specifically, we introduced STBC-TD, MMSE-SVD, and blind SLM. Mathematical signal representations for STBC-TD and MMSE-SVD in the presence of CCI from adjacent macro-cells and those for blind SLM when using STBC-TD were given. We have confirmed the effectiveness of CDAT by Monte-Carlo computer simulation. It was shown that the distributed antenna small-cell network can significantly improve the link capacity compared to centralized antenna network.

STBC-TD provides much higher cell-edge user capacity than MMSE-SVD although the latter provides much higher capacity for a user near distributed antenna (i.e., under a good channel condition). Therefore, adaptive switching between STBC-TD and MMSE-SVD achieves good capacity over an entire macro-cell area. This is left as our future study. In this paper, we assumed perfect knowledge of CSI. The impact of imperfect CSI on the performance of the proposed CDAT techniques and its countermeasure are left as our important future study. Finally, the application of blind SLM to the OFDM downlink transmission using MMSE-SVD and the computational complexity reduction of blind SLM are also left as our future study.

In our paper, independent fading was assumed for a different UE antenna. This is a reasonable assumption for a network utilizing high frequency band (e.g., above 3 GHz) which is expected to be used [5], [23] since the half carrier-wavelength becomes shorter than 5 cm and hence, UE can be equipped with at least two antennas. However, to improve the transmission performance, more than two antennas need to be used at UE. This makes the UE antenna separation less than the half carrier-wavelength. As a consequence, fading channels observed on different UE antennas become correlated. The impact of fading correlation on CDAT transmission performance is left as an important future study.

## Acknowledgement

The results presented in this paper have been achieved by "The research and development project for realization of the fifth-generation mobile communications network" commissioned to Tohoku University by The Ministry of Internal Affairs and Communications (MIC), Japan.

### References

[1] D. Astély, E. Dahlman, A. Furuskyr, Y. Jading, M. Lindstrym, and S. Parkvall, "LTE: The evolution of mobile broadband," IEEE Commun. Mag., vol.47, no.4, pp.44–51, April 2009.
[2] NTT DOCOMO Technical Journal, vol.17, no.2, Oct. 2015.
[3] Y. Kishiyama, A. Benjebbour, T. Nakamura, and H. Ishii, "Future steps of LTE-A: Evolution toward integration of local area and wide area systems," IEEE Wireless Commun., vol.20, no.1, pp.12–18, Feb. 2013.
[4] M. Sawahashi, Y. Kishiyama, A. Morimoto, D. Nishikawa, and M. Tanno, "Coordinated multipoint transmission/reception techniques for LTE-advanced [coordinated and distributed MIMO]," IEEE Wireless Commun., vol.17, no.3, pp.26–34, June 2010.
[5] C.X. Wang, F. Haider, X. Gao, X.H. You, Y. Yang, D. Yuan, H. Aggoune, H. Haas, S. Fletcher, and E. Hepsaydir, "Cellular architecture and key technologies for 5G wireless communication networks," IEEE Commun. Mag., vol.52, Issue 2, pp.122–130, Feb. 2014.
[6] R&D for radio resource expansion in fiscal year 2015 (in Japanese), www.soumu.go.jp/menu_news/s-news/01kiban09_02000169.html
[7] F. Adachi, K. Takeda, T. Obara, T. Yamamoto, and H. Matsuda, "Recent advances in single-carrier frequency-domain equalization and distributed antenna network," IEICE Trans. Fundamentals, vol.E93-A, no.11, pp.2201–2211, Nov. 2010.
[8] F. Adachi, K. Takeda, T. Yamamoto, R. Matsukawa, and S. Kumagai, "Recent advances in single-carrier distributed antenna network," Wireless Commun. Mobile Comput., vol.11, no.12, pp.1551–1563, Dec. 2011.
[9] F. Adachi, W. Peng, T. Obara, T. Yamamoto, R. Matsukawa, and M. Nakada, "Distributed antenna network for gigabit wireless access," Int. J. Electron. Commun. (AEUE), vol.66, no.6, pp.605–612, Aug. 2012.
[10] H. Miyazaki and F. Adachi, "Distributed antenna selection for OFDM space-time block coded diversity," 2016 IEEE 84th Veh. Technol. Conf. (VTC2016-Fall), Montréal, Canada, Sept. 2016.
[11] H. Miyazaki and F. Adachi, "Effect of macro-cell cooperation on distributed antenna space-time block coded diversity," IEICE Technical Report, RCS2015-273, Dec. 2015 (in Japanese).
[12] S. Kumagai and F. Adachi, "Joint Tx/Rx MMSE filtering for single-carrier MU-MIMO uplink," Proc. 12nd IEEE VTS Asia Pacific Wireless Communication Symposium (APWCS 2015), RS10: Multi-Antenna Technologies, Singapore, Aug. 2015.
[13] S. Kumagai and F. Adachi, "Effect of joint Tx/Rx cooperative signal processing on downlink broadband MU-MIMO transmissions in distributed antenna network," IEICE Technical Report, RCS2015-274, Dec. 2015 (in Japanese).
[14] S. Kumagai, S. Yoshioka, and F. Adachi, "Joint Tx/Rx filtering for distributed antenna network uplink with single-carrier MU-MIMO," IEICE Technical Report, RCS2014-355, March 2015 (in Japanese).
[15] Y. Seki and F. Adachi, "Downlink MMSE-SVD joint Tx/Rx filtering for distributed antenna small-cell network under multi-cell environment," IEICE Technical Report, RCS2016-153, Oct. 2016 (in Japanese).
[16] A. Boonkajay and F. Adachi, "Low-PAPR joint transmit/received SC-FDE transmission using time-domain selected mapping," Proc. Asia-Pacific Conference on Communications (APCC 2014), pp.248–253, Pattaya, Thailand, Oct. 2014.
[17] A. Boonkajay and F. Adachi, "A blind selected mapping technique for low-PAPR single-carrier signal transmission," Proc. Int. Conf. Info. Commun. and Signal Proc. (ICICS 2015), Singapore, Dec. 2015.
[18] A. Boonkajay and F. Adachi, "A blind polyphaser time-domain selected mapping for filtered single-carrier signal transmission," 2016 IEEE 84th Veh. Technol. Conf. (VTC2016-Fall), Montréal, Canada, Sept. 2016.
[19] A. Boonkajay and F. Adachi, "Blind selected mapping techniques for space-time block coded filtered single-carrier signals," Proc. 13th IEEE VTS Asia Pacific Wireless Communications Symposium (APWCS 2016), C4: Signal Processing for Communications II, Tokyo,

Japan, Aug. 2016.
[20] W.C. Jakes, Jr., Ed., Microwave Mobile Communications, Wiley, New York, 1974.
[21] F. Adachi, "Challenges toward spectrum-energy efficient mobile wireless networks," IEICE Tech. Report, CS2015-19, July, 2015 (in Japanese).
[22] A.A.M. Saleh, A.J. Rustako, and R.S. Roman, "Distributed antennas for indoor radio communications," IEEE Trans. Commun., vol.35, no.12, pp.1245–1251, Dec. 1987.
[23] DOCOMO 5G White Paper, 5G radio access: requirements, concept and technologies, July 2014 (https://www.nttdocomo.co.jp/english/corporate/technology/whitepaper_5g/).
[24] S.M. Alamouti, "A simple transmit diversity technique for wireless communications," IEEE J. Sel. Areas Commun., vol.16, no.8, pp.1451–1458, Oct. 1998.
[25] W. Su, X.G. Xia, and K.J. R Liu, "A systematic design of high-rate complex orthogonal space-time block codes," IEEE Commun., Lett., vol.8, no.6, pp.380–382, June 2004.
[26] H. Tomeba, K. Takeda, and F. Adachi, "Space-time block coded joint transmit/receive diversity in a frequency-nonselective Rayleigh fading channel," IEICE Trans. Commun., vol.E89-B, no.8, pp.2189–2195, Aug. 2006.
[27] K. Takeda, T. Itagaki, and F. Adachi, "Application of space-time transmit diversity to single-carrier transmission with frequency-domain equalization and receive antenna diversity in a frequency-selective fading channel," IEE Proc. Commun., vol.151, no.6, pp.627–632, Dec. 2004.
[28] H. Tomeba, K. Takeda, and F. Adachi, "Space-time block coded-joint transmit/receive antenna diversity using more than 4 receive antennas," Proc. 2008 IEEE 68th Veh. Technol. Conf. (VTC2008-Fall), Calgary, Canada, Sept. 2008.
[29] R. Matsukawa, T. Obara, and F. Adachi, "Frequency-domain space-time block coded transmit/receive diversity for single-carrier distributed antenna network," IEICE Commun. Express (ComEX), vol.2, no.4, pp.141–147, April 2013.
[30] J.G. Proakis and M. Salehi, Digital Communications, 5th ed., McGraw-Hill, 2008.
[31] T. Yamamoto, K. Takeda, and F. Adachi, "Training sequence-aided QRM-MLD block signal detection for single-carrier MIMO spatial multiplexing," Proc. IEEE Int. Conf. on Commun. (ICC 2011), Kyoto, Japan, June 2011.
[32] K. Ozaki, A. Nakajima, and F. Adachi, "Frequency-domain eigenbeam-SDM and equalization for single-carrier transmissions," IEICE Trans. Commun., vol.E91-B, no.5, pp.1521–1530, May 2008.
[33] Q. Spencer, A. Swindlehurst, and M. Haardt, "Zero-forcing methods for downlink spatial multiplexing in multiuser MIMO channels," IEEE Trans. Signal Process., vol.52, no.2, pp.461–471, Feb. 2004.
[34] T. Sada, J. Webber, T. Nishimura, T. Ohgane, and Y. Ogawa, "A generalized approach to block diagonalization for multiuser MIMO downlink," Proc. 2010 IEEE 21st Int. Symp. on Personal Indoor and Mobile Radio Commun. (PIMRC), pp.504–509, Istanbul, Turkey, Sept. 2010.
[35] A. Goldsmith, Wireless Communication, Cambridge University Press, 2005.
[36] D. Tse and P. Viswanath, Fundamentals of wireless communication, Cambridge University Press, 2005.
[37] A. Boonkajay, T. Obara, T. Yamamoto, and F. Adachi, "Excess-bandwidth transmit filtering based on minimization of variance of instantaneous transmit power for low-PAPR SC-FDE," IEICE Trans. Commun., vol.E98-B, no.4, pp.673–685, April 2015.
[38] A. Boonkajay and F. Adachi, "Selected mapping technique for reducing PAPR of single-carrier signals," Wireless Commun. Mobile Comput., vol.16, no.16, pp.2509–2522, Nov. 2016.

**Fumiyuki Adachi** received the B.S. and Dr. Eng. degrees in electrical engineering from Tohoku University, Sendai, Japan, in 1973 and 1984, respectively. In April 1973, he joined NTT and conducted various types of research related to digital cellular mobile communications. From July 1992 to December 1999, he was with NTT DoCoMo, Inc., where he led a research group on W-CDMA wireless access for 3G systems. Since January 2000, he has been with Tohoku University, Sendai, Japan. He was a full professor until March 2016 and is now a specially appointed professor for research.

**Amnart Boonkajay** received the B.E. degree in telecommunications engineering from Sirindhorn International Institute of Technology (SIIT), Thammasat University, Thailand in 2010, and Ph.D. degree in communications engineering from Tohoku University, Japan in 2016. He is currently working as a research fellow at Research Organization of Electrical Communication, Tohoku University. His research interests are based on wireless communications physical layer including transmit and receive signal processing.

**Yuta Seki** received his B.S. degree in Electrical, Information and Physics Engineering in 2002 and M.S. degree in communications engineering, in 2004, respectively, from Tohoku University, Sendai Japan. Since April 2004, he has been with Panasonic Corporation. He is currently working as an Industry-Government-Academia Collaboration researcher at Research Organization of Electrical Communication (ROEC), Tohoku University.

**Tomoyuki Saito** received the B.E. and M.E. degrees in electrical and electronic engineering from Iwate University, Morioka, Japan, in 2006 and 2008, respectively. Since April 2008, he has been with NEC communication systems Ltd. He is currently working at Research Organization of Electrical Communication (ROEC), Tohoku University, as Industry-Government-Academia Collaboration researcher.

**Shinya Kumagai** received the B.E., M.E., and Ph.D. degrees in engineering from Tohoku University, Sendai, Japan, in 2011, 2013, and 2016, respectively. From April 2013 to March 2016, he was a Japan Society for the Promotion of Science (JSPS) research fellow. He is currently with Fujitsu Laboratories Ltd. He was a recipient of the 2012 IEICE RCS (Radio Communication Systems) Outstanding Research Award.

**Hiroyuki Miyazaki** received his B.S., M.S. and Ph.D. degrees in engineering from Tohoku University, Sendai Japan, in 2011, 2013 and 2016, respectively. He was a Japan Society for the Promotion of Science (JSPS) research fellow from April 2014 to March 2016. Currently, he is with NTT Docomo Inc. His research interests include space-time block coding for mobile communication systems. He was a recipient of 2013 IEICE RCS (Radio Communication Systems) Active Research Award.